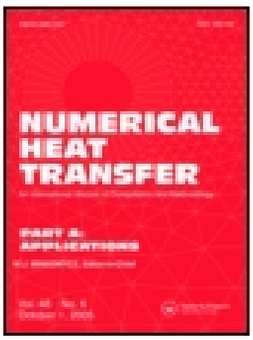

Numerical Heat Transfer, Part A: Applications

ISSN: 1040-7782 (Print) 1521-0634 (Online) Journal homepage: http://www.tandfonline.com/loi/unht20

TRANSIENT THERMAL PERFORMANCE OF AXIALLY AND RADIALLY DILUTED NUCLEAR FUEL CELLS

F. Moukalled , R. Nuwayhid & I. Lakkis

To cite this article: F. Moukalled , R. Nuwayhid & I. Lakkis (1995) TRANSIENT THERMAL PERFORMANCE OF AXIALLY AND RADIALLY DILUTED NUCLEAR FUEL CELLS, Numerical Heat Transfer, Part A: Applications, 28:2, 231-252, DOI: 10.1080/10407789508913743

To link to this article: http://dx.doi.org/10.1080/10407789508913743

Published online: 02 Mar 2007.

TRANSIENT THERMAL PERFORMANCE OF AXIALLY AND RADIALLY DILUTED NUCLEAR FUEL CELLS

F. Moukalled, R. Nuwayhid, and I. Lakkis
Faculty of Engineering and Architecture, Mechanical Engineering Department, American University of Beirut, Beirut, Lebanon

A numerical investigation is presented of steady and unsteady heat transfer in axially and radially diluted nuclear fuel rods. The transient performance is assumed to follow a sudden and complete loss of coolant starting from steady state operation. Steady state conditions are obtained from solving numerically a conjugate conduction problem in the fuel rod and a turbulent forced convection problem in the coolant section. To model turbulence, the mixing length model is used. Dilution is accomplished by adding high thermal property materials, either axially or radially, to the original fuel rods with the intention of increasing the time delay before melting of the reactor in case of loss of coolant. The effects of the amount, distribution, and material of added diluent on steady and unsteady heat transfer are studied. Results indicate that axial dilution has negligible influence on the thermal performance of the reactor. Radial dilution, however, holds great promise and shows a reduction in the maximum wall and fuel temperatures under steady operation and a substantial increase in the time delay before melting under transient conditions. The value of this time delay increases as the amount of added diluent is increased. Moreover, the distribution of the added diluent is shown to have small effects on the steady and unsteady performance of the reactor, while the type of diluent material is found to affect the transient performance only.

INTRODUCTION

This article deals with predicting the transient thermal performance of axially and radially diluted nuclear fuel cells. The motivation behind the work is the growing concern for safety in the nuclear industry. Experience has shown that engineered safeguards should not be relied upon too heavily and, rather, that dependence should be more on the so-called "inherent safety" features of reactors [1]. The analysis undertaken here is along these lines and is involved with studying, in case of loss of coolant, the possibility for a "diluted" fuel rod to absorb heat for a longer time before ultimately melting. The class of reactors under consideration is the gas-cooled fast reactor (GCFR), for which the design-based accident is considered to be a depressurization event [2–5]. If depressurization were fast or if the core was to somehow become isolated from the boilers, then the value of having in-core heat sinks becomes apparent. If, further, the depressurization were

Received 11 May 1994; accepted 12 December 1994.

The financial support provided by the University Research Board of the American University of Beirut through grant 48816 is gratefully acknowledged.

Address correspondence to Dr. F. Moukalled, Department of Mechanical Engineering, Faculty of Engineering and Architecture, American University of Beirut, P. O. Box 11-0236, Beirut, Lebanon.

Numerical Heat Transfer, Part A, 28:231–252, 1995

1040–7782/95 $10.00 + .00

NOMENCLATURE

a	ratio of added diluent volume to total fuel rod volume
b	ratio of central to total diluent cross-sectional areas
d_c, D_c	dimensional and dimensionless outer diameters of the coolant annulus
d_{D1}, D_{D1}	dimensional and dimensionless diameters of central diluent strip
d_{D2}, D_{D2}	dimensional and dimensionless outer diameters of diluent shell
d_f, D_f	dimensional and dimensionless outer diameters of outer fuel shell
d_{VD}	Van Driest factor
d_{fl}, D_{fl}	dimensional and dimensionless outer diameters of inner fuel shell
d_o	outer diameter of the rod
h	heat transfer coefficient
k_f, k_s	fluid and solid thermal conductivities
K	solid to fluid thermal conductivity ratio ($= k_s/k_f$)
l	mixing length
l_D, L_D	dimensional and dimensionless lengths of a diluent part
L, L_r	dimensional and dimensionless lengths of the fuel rod
l_n	Nikuradse-type mixing length
ND	number of added diluent parts
Nu	Nusselt number ($= hd_o/k_f$)
p, P	dimensional and dimensionless pressures
Pe	Péclet number
q_v	heat source per unit volume
r	radial coordinate
R_d	radial location of diluent shell
Re	Reynolds number ($= \rho u d_o/\mu_l$)
St	Stanton number
t, t^*	dimensional and dimensionless times
T	temperature
u, U	dimensional and dimensionless axial components of velocity
x, X	dimensional and dimensionless axial coordinates
y	distance from wall
α	solid thermal diffusivity ($= k_s/\rho c_p$)
ϵ_H	turbulent thermal diffusivity
η	dimensionless radial coordinate ($= r/d_o$)
θ	dimensionless temperature [$= (T - T_{in})/(q_v d_0^2/k_f)$]
θ_b	dimensionless bulk temperature [$= (T_b - T_{in})/(q_v d_0^2/k_f)$]
θ_w	dimensionless rod wall temperature [$= (T_w - T_{in})/(q_v d_0^2/k_f)$]
μ_l, μ_t	laminar and turbulent viscosities
ρ	density
τ_w	wall shear stress

Subscripts

b	bulk property
f	fluid property
in	condition at inlet
max	maximum value
or	original nondiluted rod
w	wall property

so rapid that the event may be viewed to be "sudden," then it may be of value to have the heat sinks as close to the fuel as possible and ultimately within the fuel rod itself. The limiting factor in the above considerations should always be that the heat sink in the form of a diluent of high thermal capacity must be in a sufficiently small amount so as to retain the "fast spectrum" character of the core [3, 4]. With this in mind, no attempt is made here to ascertain the neutronics of the diluted core design, but merely an upper limit on the diluent-to-fuel ratio is imposed at random. A complete study should consist of investigating the nuclear properties of the fuel, then studying and improving the heat transfer characteristics, then assessing the nuclear properties, and so forth, until convergence of a design is reached as a compromise between the nuclear and the heat transfer requirements. Thus, it is stressed here that this work is intended to test, *from a heat transfer point of view*, the above stated idea of adding diluents (high thermal property materials)

to the fuel rod of a GCFR in order to have in-core heat sinks so as to enhance the reactor safety by increasing its time delay before melting in case of accidental loss of coolant.

The problem is modeled and reduced to that of predicting the heat transfer characteristics of turbulent fluid flow around a longitudinally and radially conducting slender rod with periodic internal heat generation. The heat produced in the "average" rod by the fission chain reaction is assumed to be radially independent with an axial cosine distribution [6]. The analysis is conducted for both steady and transient performance in case of a sudden and complete loss of coolant before shutting the reactor down. Initial conditions for the transient heat conduction problem in the fuel rod are obtained from the steady state performance of the coolant-rod problem. Due to the unavailability of any experimental or numerical data related to the problem, numerical results of the simple problem shown in Figure 1*a* are compared with analytical solutions obtained using several empirical models.

GOVERNING EQUATIONS AND BOUNDARY CONDITIONS

The physical situations under consideration, illustrated schematically in Figures 1*b* and 1*c*, represent the turbulent convection of a fluid around longitudinally and radially conducting slim rods with periodic internal heat generation. In Figure 1*b*, longitudinal diluent strips are added at several radii to the original fuel rod, while in Figure 1*c*, diluent strips are added to the original fuel rod at several axial locations. The coolant is assumed to enter the annulus with uniform temperature and velocity profiles of values T_{in} and u_{in}, respectively. Moreover, the properties of the steady, two-dimensional axisymmetric flow are temperature dependent; their expressions are displayed in Table 1. The pressure of the coolant, chosen to be carbon dioxide, at the inlet to the annulus is assumed to be uniform and equal to

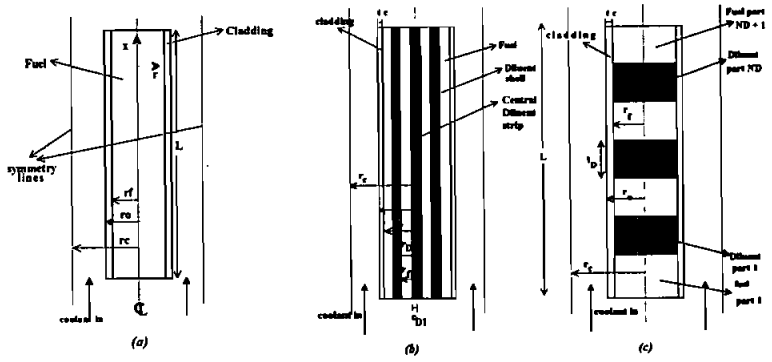

Figure 1. (*a*) Physical situation for typical coolant-fuel rod cell. (*b*) Schematic of a radially diluted fuel cell. (*c*) Schematic of an axially diluted fuel cell.

Table 1. Properties of coolant, fuel, cladding, and tested diluents (SI units)

	k	ρ
CO_2	$7.1 \times 10^{-5}\mathrm{T} - 6.16 \times 10^{-4}$	$21{,}173.16/T$
UO_2	$7.54 - 0.0053T + 1.3 \times 10^{-6}T^2$	10,400
Stainless steel	$0.012T + 8.22$	7,900
Graphite	1.51	2,250
Al_2O_3	0.30	3,965
SiC	0.42	3,217
	c_p	μ
CO_2	$k/c_p = 3.36 \times 10^{-5}\ln \mathrm{T} - 1.76 \times 10^{-4}$	$6.65 \times 10^{-6} + 3.56 \times 10^{-8}T$
UO_2	$228 + 0.274T - 0.00027T^2 + 9.2 \times 10^{-8}T^3$	—
Stainless steel	$0.25T + 411.75$	—
Graphite	$931.8 + 0.91T - 4.075 \times 10^7/T^2$	—
Al_2O_3	$906.71 + 0.37T - 2.15 \times 10^7/T^2$	—
SiC	$928.31 + 0.30T - 2.97 \times 10^7/T^2$	—

40 bars, a typical value of the pressure inside the pressurized vessel containing the reactor core [6].

In order to reduce the number of parameters involved, the following dimensionless variables are defined:

$$X = \frac{x}{d_o} \qquad \eta = \frac{r}{d_o} \qquad U = \frac{u}{u_{in}} \qquad V = \frac{v}{u_{in}} \qquad P = \frac{p}{\rho u_{in}^2}$$
$$\theta = \frac{T - T_{in}}{q_v d_o^2/k_f} \qquad t^* = \frac{t}{d_o^2/\alpha}c \tag{1}$$

Furthermore, axial diffusion in the fluid is neglected due to the high value of Péclet number in turbulent flow ($\gg 50$). With this assumption, the governing conservation equations may be expressed in parabolic form and are detailed in the following sections.

MOMENTUM EQUATION AND TURBULENCE MODEL

The momentum equation for the coolant in the annulus, in dimensionless form, may be written as

$$U\frac{\partial U}{\partial X} + V\frac{\partial U}{\partial \eta} = -\frac{\partial P}{\partial X} + \frac{1}{\mathrm{Re}_{in}}\frac{1}{\eta}\frac{\partial}{\partial \eta}\left[\eta\left(1 + \frac{\mu_t}{\mu_l}\right)\frac{\partial U}{\partial \eta}\right] \tag{2}$$

where μ_l and μ_t are the laminar and turbulent viscosities, respectively. Moreover, the boundary conditions used for solving the above equation are

$$U=1 \qquad X=0 \tag{3a}$$

$$\partial U/\partial\eta=0 \qquad \eta = D_c/2 \tag{3b}$$

$$U=0 \qquad \eta = 0.5 \tag{3c}$$

The turbulent viscosity μ_t is calculated using Prandtl's mixing length model [7]. For simple annulus flows, such as those considered in this study, it has been shown to be adequate [8]. In this model, μ_t is evaluated in terms of the mixing length and the local velocity gradient. A commonly used representation for μ_t is

$$\mu_t = \rho l^2 \left|\frac{du}{dy}\right| \tag{4}$$

where l is the mixing length at a point situated at a distance y from the wall of the fuel rod ($y = r - d_o/2$) and is represented as the product of a Nikuradse-type mixing length l_n [9] and a Van Driest factor d_{VD} [10], i.e.,

$$l = l_n\, d_{VD} \tag{5}$$

For turbulent annulus flow between inner diameter d_o and outer diameter d_c, l_n and d_{VD} are given by

$$\frac{l_n}{(d_c - d_o)/2} = 0.14 - 0.08\left[1 - \frac{y}{(d_c - d_o)/2}\right]^2 - 0.06\left[1 - \frac{y}{(d_c - d_o)/2}\right]^4$$

$$d_{VD} = 1 - \exp\left[-\left(\frac{\rho y}{26\mu_l}\right)\sqrt{\frac{\tau_w}{\rho}}\right] \tag{6}$$

where τ_w is the local shear stress on the pipe wall. By combining Eqs. (5) and (6), the mixing length l and, consequently, μ_t (Eq. (4)) are completely specified.

ENERGY EQUATIONS

The conservation of energy equation for the axisymmetric parabolic flow problem, in dimensionless form, can be written as

$$U\frac{\partial\theta}{\partial X} + V\frac{\partial\theta}{\partial\eta} = \frac{1}{\mathrm{Pe}}\frac{1}{\eta}\frac{\partial}{\partial\eta}\left[\eta\left(1 + \frac{\epsilon_H}{\alpha}\right)\frac{\partial\theta}{\partial\eta}\right] \tag{7}$$

subject to the following initial and boundary conditions:

$$\left(\frac{\partial\theta}{\partial\eta}\right)_{w(f)} = K\left(\frac{\partial\theta}{\partial\eta}\right)_{w(s)} \qquad \eta = 0.5 \tag{8a}$$

$$\frac{\partial\theta}{\partial\eta} = 0 \qquad \eta = D_c/2 \tag{8b}$$

$$\theta = 0 \qquad X = 0 \tag{8c}$$

The energy equation for the steady and unsteady heat conduction problems in the fuel rod is

$$\frac{\partial\theta}{\partial t^*} = K\frac{1}{\eta}\frac{\partial}{\partial\eta}\left(\eta\frac{\partial\theta}{\partial\eta}\right) + K\frac{\partial^2\theta}{\partial X^2} + 1 \tag{9}$$

where K is the solid to fluid thermal conductivity ratio. The applicable initial and boundary conditions of the conduction energy equation are

$$\frac{\partial\theta}{\partial\eta} = 0 \qquad \eta = 0 \tag{10a}$$

$$\frac{\partial\theta}{\partial X} = 0 \qquad X = 0 \qquad X = L_r \tag{10b}$$

$$\theta = \theta_w(X) \qquad \eta = 0.5 \tag{10c}$$

(for steady state performance)

$$\frac{\partial\theta}{\partial\eta} = 0 \qquad \eta = 0.5 \tag{10d}$$

(for transient performance), where $\theta_w(X)$ is the temperature distribution along the wall of the fuel rod, which is not known a priori but is determined from solving the convection energy equation. Moreover, $\theta_w(X)$ and $(\partial\theta/\partial\eta)_w$ provide the coupling between the convection and conduction problems. Furthermore, due to the lack of any better information, the wall of the fuel rod in contact with the coolant during steady performance is assumed, under transient conditions, to be insulated. Thus, results generated in this paper simulate the worst probable situation that could arise during an accident. As such, any improvement in the performance of the fuel rod is expected to further magnify if this condition is relaxed.

FUEL ROD PARAMETERS AND CONFIGURATIONS

Due to the large number of parameters involved in the problem, the effect of varying only selected parameters is studied. The parameters fixed throughout the

Table 2. Parameters fixed throughout the analysis

Parameter	Value
Coolant annulus cross-sectional area, m^2	6.77×10^{-5}
Cladding thickness, m	0.00035
Fuel cross-sectional area, m^2	3.85×10^{-5}
Fuel length, m	1.5
Energy produced in the fuel, W	25,189
Coolant inlet temperature, K	525
Coolant inlet axial velocity, m/s	30

analysis along with their values are presented in Table 2. Properties of the working fluid (CO_2), fuel (UO_2), cladding (stainless steel), and diluents are shown in Table 1.

Axial dilution of the fuel rod is accomplished by adding strips of material with high thermal properties to the original fuel rod at several axial locations. The added diluent parts are identical, their number is ND, each is of length l_d and is equally spaced (Figure 1*c*). In testing axially diluted rods, the amount of added diluent is kept constant for all analyzed cases, and its total length is half the length of the original fuel rod (i.e., ND $l_d = 0.5L_{or}$). Axial dilution is tested for only one diluent material (natural UO_2 with no enrichment) for reasons that will become apparent later. Moreover, the heat source in each fuel part is assumed to have a local axial cosine distribution (with center of the part as the local origin) such that it is equal to the heat source obtained from the global distribution in the case of no dilution at the same axial distance and location.

In radially diluting a fuel rod, the following two procedures are adopted: (1) central dilution and (2) central and strip dilution. In both cases, the diluent extends axially over the entire fuel rod. With central and strip dilution, half of the diluent material is placed at the central axis and the other half at a distance of $R_d = 0.7$. Here tests are conducted for four diluent materials.

SOLUTION PROCEDURE AND COMPUTATIONAL DETAILS

For the conjugate heat transfer problem, the fluid momentum and energy equations, Eqs. (2) and (7), are solved numerically using the parabolic calculation procedure of Patankar and Spalding [11]. This is a fully implicit, marching-type solution procedure, proceeding from the inlet location ($X = 0$) to the exit of the annulus ($X = L_r$). The steady and unsteady heat conduction problems in the fuel rod, Eq. (9), are solved by the elliptic finite volume method described by Patankar [12].

The conjugate conduction-convection coupling is solved via an iterative approach in which the energy and momentum equations for the fluid and the energy equation for the fuel rod are solved consecutively. To start the first iteration, the fuel energy equation, Eq. (9), is solved by imposing a guessed value of $\theta_w(X)$ as the boundary condition needed in Eq. 10*c*. The solution obtained is fed

into the fluid energy equation, Eq. (7), via the term $(\partial\theta/\partial\eta)_{\eta=0.5}$ (Eq. 8*a*), which is solved, after solving the fluid momentum equation, to obtain updated values for $\theta_w(X)$. The updated $\theta_w(X)$ is used to initiate the second iteration, and the fuel rod energy equation is solved again. This procedure is continued until convergence to at least four significant figures is reached.

The computational task is fairly demanding due to the periodic geometry (in the case of axial dilution) and the iterative nature of the adopted solution procedure. In the case of axial dilution, the thermal boundary layer developing each time a fuel segment is encountered necessitates the use of a smaller forward step size. The flow computations are performed with 175 grid points scanning the annulus cross section, $0.5 \leq \eta \leq D_c/2$, and clustering near the rod wall. In the axial direction, a uniform step size of value 10^{-3} for all radially diluted rods and 10^{-4} for all axially diluted rods is used. A total of 1500 or 22,500 points in the streamwise direction are employed, and the 1500×175 or $22{,}500 \times 175$ mesh systems for the radially and axially diluted rods, respectively, are found to be adequate for producing grid independent results. For the solution of the fuel rod conduction equation for both steady and unsteady situations, a mesh is employed consisting of 71 grid points in the axial direction for radial dilution, and 105 grid points for axial dilution. In the radial direction, 54 grid points are used for both types of dilution. When transferring data from the steady condition problem to the convection problem, linear interpolation was employed. The step size in the flow problem was sometimes modified to allow for the radial faces of the conduction control volume to be identical to streamwise positions in the flow solution, so that the transfer of information from the flow problem to the conduction problem is made direct and easier.

RESULTS AND DISCUSSION

As mentioned before, two sets of illustrative cases are considered. The first set corresponds to axial dilution, where four values of ND (ND = 1, 2, 3, and 4) are considered. This selection explores the effect of increasing the number of added diluent parts ND on the thermal performance of the fuel rod. The second set consists of a wider variety of cases chosen to investigate radial dilution, whereby three trends of analysis are followed. The first trend is varying a, the ratio of the volume of added diluent to total fuel rod volume, where the following six values are considered: 0, 0.1, 0.2, 0.3, 0.5, and 0.7. The parameter a reflects the effectiveness of the heat sink, represented by the diluent, as compared with the heat source represented by the fuel. The second trend is the way the diluent is radially distributed. Only two possible distributions are investigated; the first locates all the diluent at the central axis of the rod, so that $b = 1$ and $R_d = 0$, whereas the second locates half of the diluent material at the central axis ($b = 0.5$) and the other half at a radius that is equal to 0.7 times the outer fuel strip radius ($R_d = 0.7$). The third trend of analysis is intended to study the effects of the diluent thermal properties. For this purpose, four materials are considered: uranium dioxide (UO_2), graphite (C), alumina (Al_2O_3), and silicon carbide (SiC). Results presented in the following sections reveal the influence on steady and unsteady heat transfer of the various parameters involved.

COMPARISON OF ANALYTICAL AND NUMERICAL RESULTS

Due to the unavailability of any experimental data related to the problem at hand, results are validated by comparing numerical steady state conduction values obtained in the original nondiluted rod against results generated analytically using various empirical turbulent models (Figure 2). The empirical models used in obtaining the heat transfer coefficients [13, 14], which do not apply completely to the case of fluid flow around a cylinder with variable heat generation, are represented by the following equations:

$$\text{Dittus-Boelter:} \quad \mathrm{St}_b = 0.023\,\mathrm{Re}_b^{-0.2}\,\mathrm{Pr}^{-0.6} \text{ (Model 1)} \tag{11a}$$

$$\text{McAdams:} \quad \mathrm{Nu}_b = 0.019\,\mathrm{Re}_b^{0.8}\,\mathrm{Pr}^{0.4} \text{ (Model 2)} \tag{11b}$$

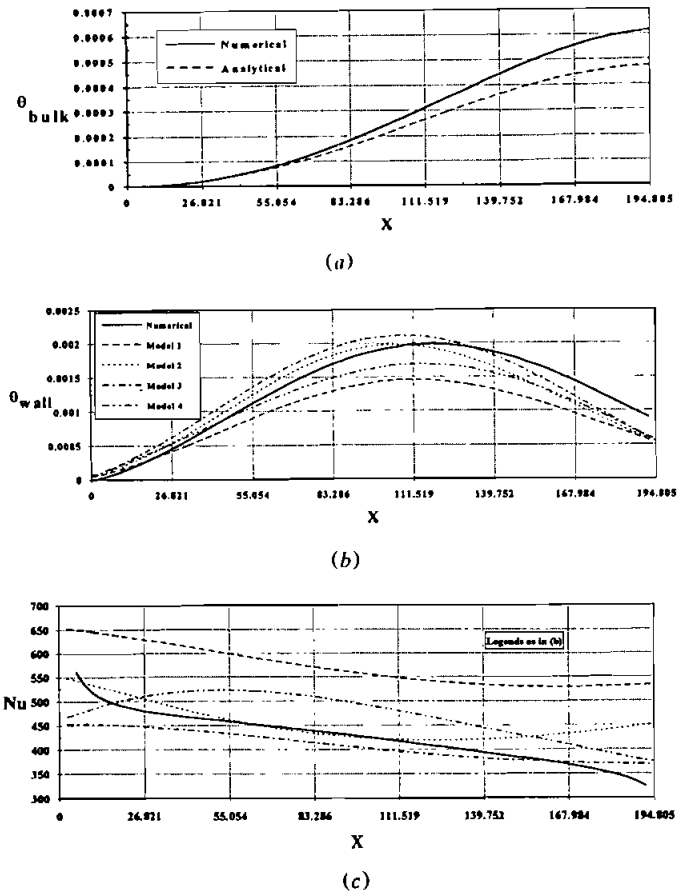

Figure 2. Comparison between numerical and analytical predictions of (*a*) coolant bulk temperature, (*b*) wall temperature, and (*c*) Nusselt number along the original fuel rod.

$$\text{Colburn:}\quad \mathrm{St_b}(m_f c_{pb}/k_b)^{2/3} = 0.023\,\mathrm{Re_b^{-0.2}}\ \text{(Model 3)} \tag{11c}$$

$$\text{Seider and Tate:}\quad \mathrm{St_b\ Pr^{2/3}}(m_w/m_b)^{0.14} = 0.027\,\mathrm{Re_b^{-0.2}}\ \text{(Model 4)} \tag{11d}$$

where $\mathrm{St} = h/\rho u c_p$ is the Stanton number. These models are applicable to turbulent fluid flow in a smooth pipe, where the variation of streamwise wall temperature and fluid properties is not anticipated precisely, for $0.5 < \mathrm{Pr} < 120$, $2000 < \mathrm{Re} < 10^7$, and $L/D > 50$, all satisfied here. Moreover, the coolant bulk temperature at the exit, used as input to the analytical solver, was determined on the basis of the simple overall energy balance without accounting for the variation of the fluid thermal capacity and did not include conduction effects in the streamwise direction. This has led to underestimating the coolant bulk temperature at the exit, as shown in Figure 2*a*. However, the general behavior is similar to that obtained numerically. Furthermore, as a result of the above approximations, the analytical distributions of wall temperatures (Figure 2*b*) and Nusselt numbers (Figure 2*c*) either underestimate or overestimate the actual situation, which is best represented through the numerical results. As shown in Figure 2*b*, the streamwise wall temperature distributions obtained using the various empirical models show the same behavior as the numerical distribution, namely, of rising to a maximum somewhere beyond the center and then decreasing all the way to the exit. Therefore, the numerical results fall in the range of results generated by the empirical models, which shows the adequacy and correctness of the numerical procedure.

STEADY CONJUGATE HEAT TRANSFER RESULTS

Axial Dilution

Bulk temperatures. The streamwise variation of the fluid bulk temperature, defined as,

$$T_b = \int_{d_o/2}^{d_c/2} \rho u (2\pi r\, dr) c_p T \Big/ \int_{d_o/2}^{d_c/2} \rho u (2\pi r\, dr) c_p \tag{12}$$

for the various values of ND are depicted in Figure 3*a*. It is noted that although the dimensionless values at an axial location are different for different values of ND, they are exactly the same at the exit. For these cases, $\theta_{b(\mathrm{exit})}$ equals to 0.0009, which yields a dimensional exit bulk temperature of nearly 770 K. For the original nondiluted rod, even though $\theta_{b(\mathrm{exit})}$ is not equal to 0.0009, because the length of the fuel rod for this case is two thirds of the axially diluted rod, the dimensional exit bulk temperature is again 770 K. Note that, since the energy produced by the fuel rod, Q, the coolant inlet velocity and temperature, and the coolant flow area are fixed throughout the analysis, the equality at the exit of the fluid bulk temperature should be expected and may be explained on the basis of the law of energy conservation; energy released by the fuel rod is equal to the energy carried by the fluid. The only noninsulated wall is the one in contact with the coolant, and therefore, no energy generated within the rod can be transferred except to the

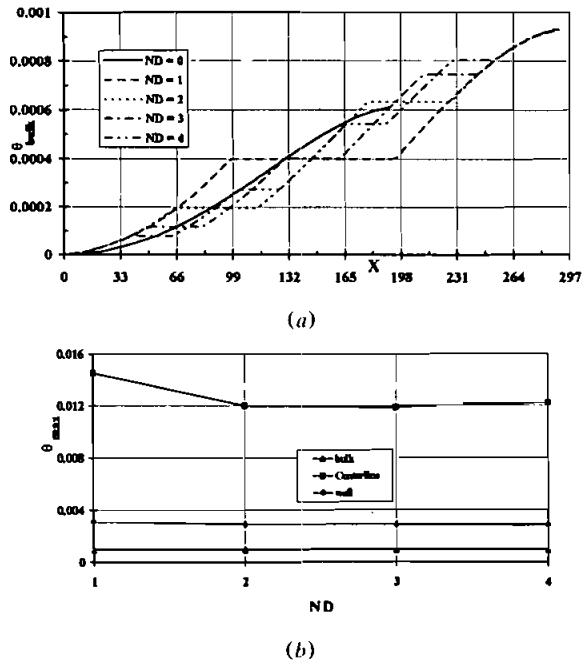

(*a*)

(*b*)

Figure 3. (*a*) Streamwise variation of the coolant bulk temperature for various axially diluted rods. (*b*) Variation of maximum bulk, wall, and fuel temperatures with ND for axially diluted rods.

fluid. Since for various values of ND the same energy is released, the same energy will be carried by the fluid and thus, the bulk temperatures at the exit should be equal.

The streamwise distribution of T_b, however, is very dependent upon ND (Figure 3*a*). The reason for that is the presence of the diluent parts in which no heat is generated and along which the increase in the bulk temperature is marginal. This marginal increase in the bulk temperature along the diluent parts implies that their wall temperature is nearly uniform and equal to T_b. Thus, the diluents are not serving the purpose for which they were added, i.e., they are not acting as in-core heat sinks, and they simply redistribute the locations where heat is convected to the fluid. Moreover, heat is not conducted effectively to the diluent parts in the fuel rod because the dominant direction of heat transfer is the radial direction due to two factors: (1) the radial dimension is very small in comparison to the axial dimension ($L_r/d_o = 292$); (2) the high radial temperature gradient in the fuel rod, the low coolant temperature, and the high turbulence mixing cause the energy generated to be convected to the coolant, leaving almost no energy to be conducted to the diluent. The temperature profiles displayed in Figure 3*b* show once more that the bulk temperature at the exit is independent of ND.

Wall and fuel temperatures. The streamwise variation of the wall temperature for the nondiluted rod is shown in Figure 4*a*. It rises from a minimum

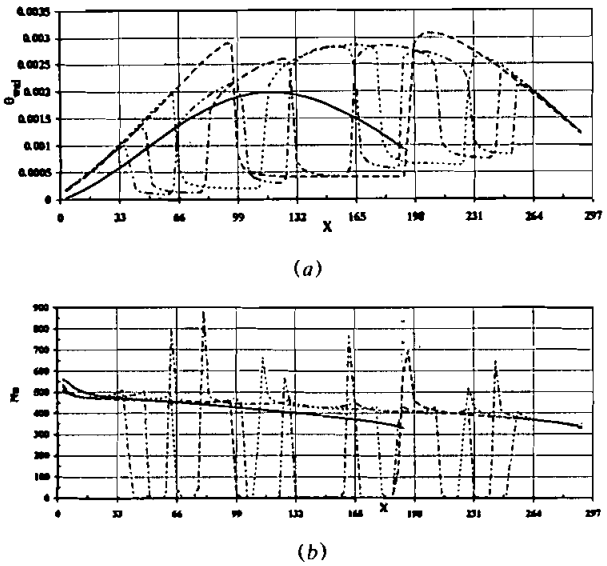

(*a*)

(*b*)

Figure 4. Axial variation of (*a*) wall temperature and (*b*) Nusselt number for various axially diluted rods. Symbols explained in Figure 3.

($\theta = 0$) at the inlet to a maximum somewhere beyond the middle of the fuel rod, and then decreases all the way to the exit. Even though the heat source has a cosine distribution that maximizes at the center, the maximum wall temperature is shifted toward the exit due to the interaction of the heat source with the convective coolant fluid of steadily increasing bulk temperature.

The same phenomenon of shifting the maximum wall temperature is revealed in the axially diluted rods (Figure 4*a*), but the existence of the diluent renders the axial wall temperature distribution different. It is first noted that the heat source distribution in a certain fuel part is the same as that for the corresponding part in the original nondiluted rod. The heat source distribution together with the steadily increasing bulk temperature, which is almost constant over a diluent part, cause the wall temperature along a fuel part to be similar to that of the corresponding part of the nondiluted rod. Moreover, the wall temperature along all diluent parts shows a common behavior of decreasing at the entrance and then maintaining a constant value until reaching the other end, after which it increases abruptly at the inlet to the adjacent fuel part. Furthermore, due to the weak axial conduction, which does not allow heat to be transferred axially a significant distance inside the diluent, the wall temperature is equal to the bulk temperature there, indicating a radial flux of zero value.

Since the length of an axially diluted rod is 1.5 times that of the nondiluted rod, the actual wall temperature for ND > 0 should be viewed as multiplied by a factor of 2/3, as was the case when bulk temperatures were compared. With this in mind, the maximum dimensionless wall temperature θ_w for the nondiluted rod is 0.002, which is approximately two thirds that of the axially diluted rod when

ND = 1 (0.0031). Referring to Figure 3*b*, the maximum wall temperature is seen to be nearly independent of ND, with a shy minimum for a value of ND between 2 and 3 due to a relatively more effective distribution of the diluent that slightly enhances axial conduction, causing a redistribution of the wall temperature with a drop in its maximum value. The maximum fuel temperature profile shows noticeable dependence on ND (Figure 3*b*). As was the case with the wall temperature, the lowest maximum fuel temperature is also obtained for a value of ND between 2 and 3.

Nusselt numbers. The local and average Nusselt numbers are calculated using the following equations:

$$\mathrm{Nu} = hd_o/k_f \qquad \mathrm{Nu}_{ave} = h_{ave}d_o/k_{f\,ave} \tag{13}$$

The streamwise variations of Nusselt number for various values of ND are presented in Figure 4*b*. The general behavior indicates two levels between which it varies. The upper level is reached when the coolant flows along a fuel part, whereas the lower level (≈ 0) is attained when the coolant flows along a diluent part. Along a fuel part, Nu reaches the upper level and decreases with increasing downstream distance until reaching a diluent part, where it drops almost abruptly to the lower level. At the entrance to a fuel part, a new thermal boundary layer is generated, which results in higher values of heat transfer coefficient due to the high heat transfer rates associated with developing boundary layers. The average values, however (not presented for compactness), are found, as expected, to be nearly equal and independent of ND (variation is in the range [294, 308]), reflecting the equality of the amount of energy transferred. The slight differences among the various values are attributed to variations in the fluid properties upon which the fluid thermal conductivity is dependent.

Radial Dilution

Bulk temperatures. The streamwise variations of the coolant bulk temperature are displayed in Figure 5*a*. In this case the dimensionless length of the domain becomes shorter as a increases due to the increase in the outer diameter d_o. The relation between the dimensional and dimensionless temperatures may be written as

$$T_b = T_{in} + \frac{4Q}{\pi L}\frac{\theta_b}{k_f} \tag{14}$$

where Q is the total energy generated by the fuel rod. From the above equation, since the rod length L is constant, the dimensionless bulk temperature θ_b gives nearly a direct reference to the dimensional bulk temperature T_b. Referring to Figure 5*a*, it is noted that the coolant bulk temperature at the exit is nearly the same for all diluent additions with a slight increase with a. This slight increase is due to the dependence of c_p and k_f on temperature. Furthermore, since

$$Q = mc_{pav}(T_{b(exit)} - T_{b(inlet)}) \tag{15}$$

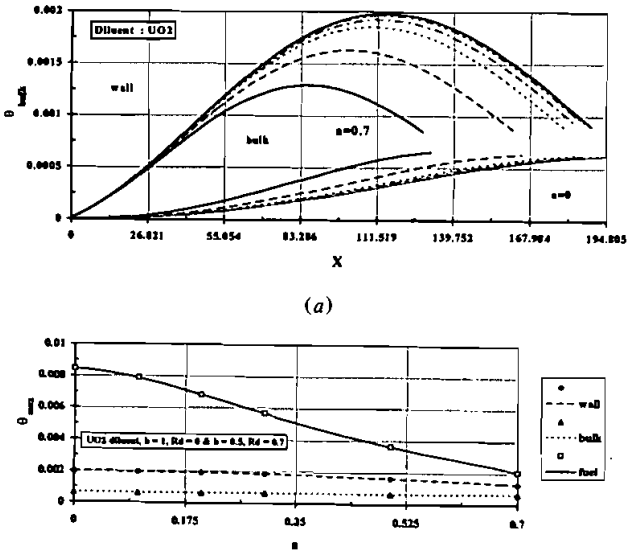

(*a*)

(*b*)

Figure 5. (*a*) Streamwise variation of the coolant bulk and wall temperatures for various radially diluted rods (a = 0, 0.1, 0.2, 0.3, 0.5, and 0.7, central dilution). (*b*) Variation of maximum bulk, wall, and fuel temperatures with a for radially diluted rods (central dilution).

$T_{b(exit)}$ may vary slightly due to variations in the coolant heat capacity. Variations of $\theta_{b(exit)}$ with a are shown comparatively with corresponding variations of maximum wall and fuel temperatures in Figure 5*b*.

The effect of redistributing the same amount of diluent, using the practices described earlier, on the coolant bulk temperature is small to the extent that it is not revealed for the highest value of a. This is because the diluent has no effect on the heat generated at a certain streamwise location, so that the corresponding energy carried by the fluid at that location is the same. Moreover, for the highest diluent addition of a = 0.7, the effect of varying the diluent material, and consequently, the diluent properties are found to be negligible.

Wall temperatures. The streamwise variation of wall temperatures (Figure 5*a*) is similar to that of the nondiluted rod discussed previously (Figure 2*a*). As depicted in Figure 5*a*, the wall temperature decreases with increasing a. This is anticipated due to the increase in the fuel rod volume and radial dimension. Since the heat conducted in the rod is directly proportional to $A\ dt/dr$ and since A and dr are increasing, dt should decrease for the same amount of heat conducted. Moreover, the streamwise uniformity of the diluent distribution renders similar streamwise behavior of wall temperature distributions for the various diluent additions (a = 0–0.7) with identical locations of maximum wall temperatures.

As mentioned before, the maximum wall temperature is the basic design temperature that should be maintained below its critical value. Increasing a results

in a significant decrease in the maximum wall temperature, as shown in Figure 5*a*. Therefore, this configuration holds great promise for inherently improving the safety of the nuclear reactor. Since the wall temperature has decreased, the nuclear reactor will be able, in case of loss of coolant accidents, to absorb its own generated heat for a longer time before melting. Furthermore, the effects of diluent distribution and diluent material on the streamwise distribution of wall temperatures are found to be negligible.

Nusselt numbers. The streamwise variation of Nu (Figure 6*a*) is similar to that of the nondiluted rod (Figure 2*c*) due to the axial uniformity of the radial diluent distribution. Moreover, average Nu values increase with increasing values of a (Figure 6*b*). To explain this behavior, reference is made to Eq. (13), where Nu is seen to be mainly dependent on d_o and h because variations in k_f are

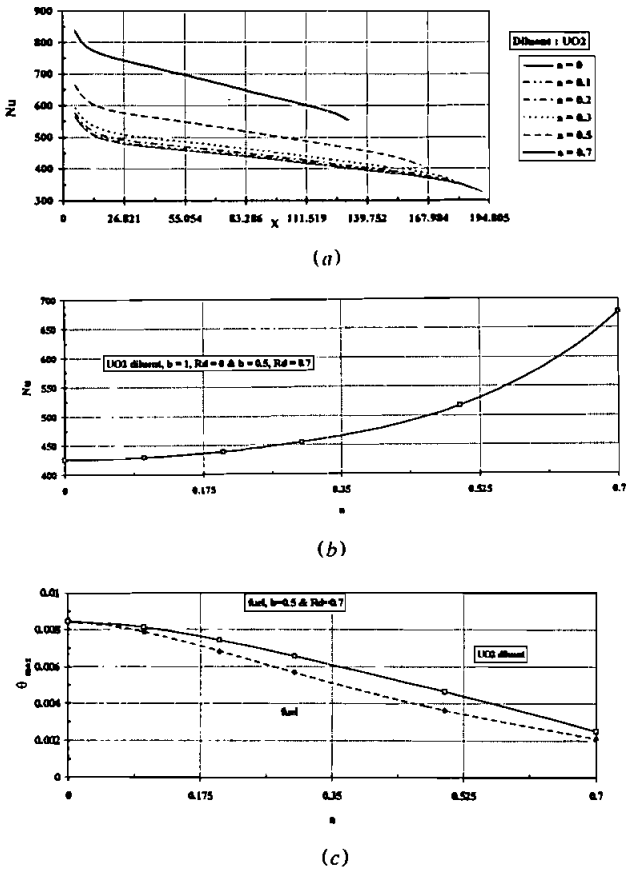

Figure 6. (*a*) Axial variation of Nusselt number for radially diluted rods (central dilution). (*b*) Variation of average Nusselt number with a for radially diluted rods (central dilution). (*c*) Variation of maximum fuel temperature with a for central and central-and-strip radial dilutions.

comparatively small. Since the values of d_o and h both increase with a, Nu should increase. The increase in the level of heat transfer coefficient can be explained by referring to its average value and the following energy balance equation:

$$Q = h_{ave} A_c (T_{w(ave)} - T_b) \tag{16}$$

As a increases, the coolant–fuel rod contact area (A_c) increases and $T_{w(ave)}$ decreases, but the rate of decrease in $T_{w(ave)}$ is much higher than the rate of increase in A_c. Therefore, since Q, the heat generated by the fuel, is constant, Eq. (16) shows that h should increase. Again, the effects of diluent distribution and material on Nu are found to be marginal.

Maximum fuel temperature. The maximum fuel temperature is found to be dependent not only on the amount of diluent added but also on the way it is distributed. Referring to Figure 6*c*, as a increases, the maximum fuel temperature decreases for both types of radial dilution. However, placing a part of the diluent away from the central axis results in fuel temperatures higher than those obtained with pure central dilution because of the higher thermal resistance induced by the diluent part, which necessitates higher temperature difference for the same heat flux. This difference is magnified as the amount of added diluent increases (i.e., a) up to a critical value ($a_c = 0.5$). Increasing a above a_c reduces $\Delta\theta_{fuel(max)}$ (difference in maximum fuel temperature for both types of radial dilution) due to the relatively large amount of added diluent.

UNSTEADY CONDUCTION HEAT TRANSFER RESULTS

The steady state results of the previous section are as the initial conditions for simulating the transient performance of the reactor core in case of a sudden loss of coolant accident. Under such conditions, the problem reduces to that of unsteady conduction heat transfer in a thermally insulated heat generating rod. The temperature in the rod is expected to increase with time, but at different rates; the temperatures in regions close to the coolant in steady state performance are expected to experience higher rates of increase than those nearer to the centerline, especially since the wall is assumed to be insulated.

It should be noted that during steady operation, even though the maximum wall temperature was lower than the maximum fuel temperature, it was closer to its limiting value (i.e., $\theta_{w\,max(s.s)}/\theta_{w(lim)} = 0.0079$ and $\theta_{fuel\ max(s.s)}/\theta_{fuel(lim)} = 0.0755$) (Figure 5*a*). The limiting dimensional wall temperature for the stainless steel cladding is the melting point, equal to 1673 K, which corresponds to a dimensionless value of $\theta_{w(lim)} = 0.0254$. (The limiting value is actually the fault temperature, which is lower than the melting temperature and beyond which the material loses its strength. However, in this work, the melting point is assumed to be the limiting temperature.) Whereas the limiting fuel temperature is 3138 K, corresponding to $\theta_{fuel(lim)} = 0.1085$. Thus, the maximum wall temperature is expected to reach its limiting value before the maximum fuel temperature.

The above speculations are confirmed by the unsteady streamwise distribution of wall (Figure 7*a*) and fuel centerline temperatures (Figure 7*b*) of the original nondiluted rod. As depicted the wall and fuel temperatures maintain the same

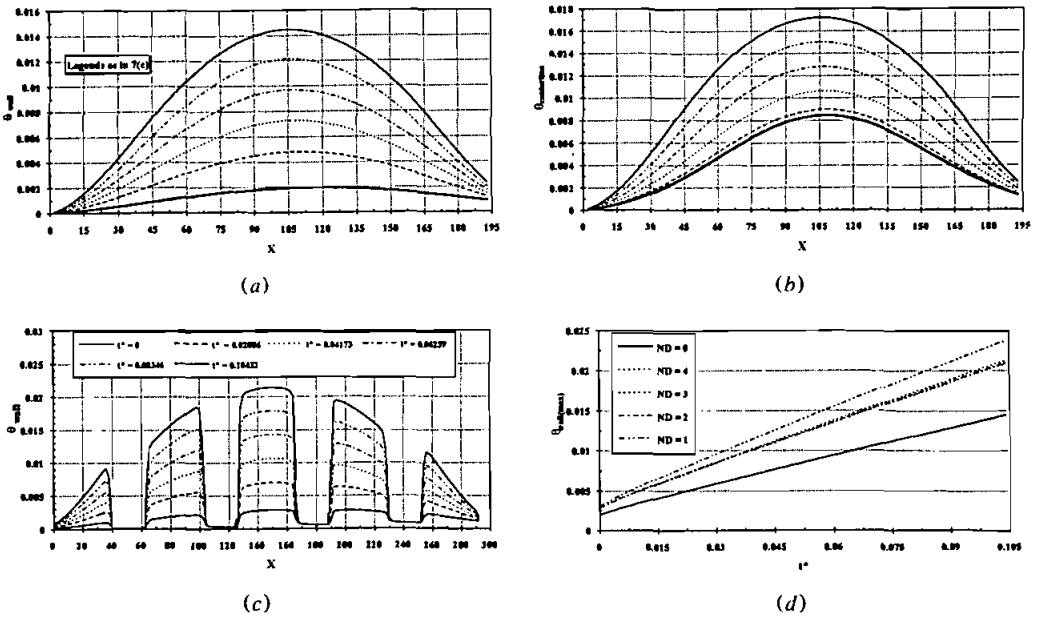

Figure 7. Transient axial distribution of (*a*) wall and (*b*) centerline temperatures in the original nondiluted fuel rod. Transient variation of (*c*) axial and (*d*) maximum wall temperatures in axially diluted rods.

shape, with a shift in the maximum toward the center, where maximum heat generation occurs. This is because the rod is insulated, convection is totally lost, and the radial direction is the dominant direction of conduction heat transfer. From Figure 7*a* and 7*b*, it is obvious that the maximum wall temperature will reach its limiting value long before the fuel centerline temperature because it is increasing at a higher rate (e.g., at $t^* = 0.1$, $\theta_{w\,max}$ increases by a factor of about 7, whereas $\theta_{fuel\,max}$ increases by a factor of 2 only). Thus attention should be directed toward maximizing the time delay before the maximum wall temperature reaches its limiting value.

Axial Dilution

Maximum wall temperature. The unsteady streamwise distribution of wall temperature is shown in Figure 7*c* for the case of ND = 4. It is noted that the wall temperature along a diluent section experiences a very slight increase in its value during unsteady performance, whereas it increases at a much higher rate along a fuel part. This is to be expected for reasons mentioned in the steady state analysis. The variation of maximum wall temperature with time for the various diluent additions is displayed in Figure 7*d*. The difference between the maximum wall temperature of the nondiluted and diluted rods is small and does not increase appreciably with time, which assures that the added diluent parts are not serving

their intended purpose and are not acting as in-core heat sinks. The slightly lower maximum wall temperature for higher ND values continues during unsteady performance.

Maximum fuel temperature. The unsteady streamwise distribution of fuel temperature (centerline temperature) is presented in Figure 8*a* for the case of ND = 4. As displayed, the unsteady behavior is similar to that of the wall temperature, but the rate of increase in temperature with time is much lower than that along the wall. Figure 8*b* shows the transient variation of the maximum fuel temperature for various diluent additions. The rate of increase in the value of $\theta_{\text{fuel(max)}}$ is initially low, but this rate increases with time. This is due to the fact that at the beginning of the unsteady performance, wall temperatures being low, a

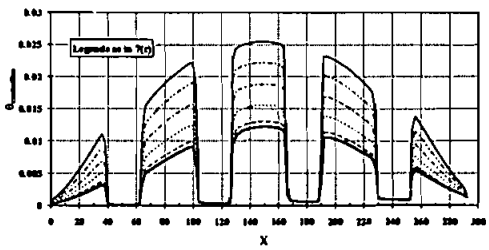

(*a*)

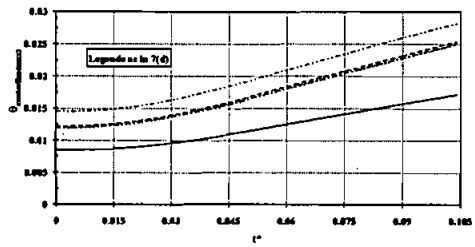

(*b*)

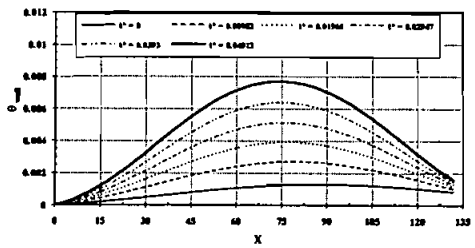

(*c*)

Figure 8. (*a*) Transient axial distribution of centerline temperature in axially diluted rods. (*b*) Variation of maximum centerline temperature with time for axially diluted rods. (*c*) Transient axial distribution of wall temperature in radially diluted rods (a = 0.7, central dilution).

large amount of the heat generated is radially conducted toward the outer wall. As time increases, wall temperatures increase, leading to lower radial conduction and thereby to higher values of fuel temperatures. Actually, this is the main reason why the maximum wall temperature increases at a rate higher than that of the fuel temperature and reaches its limiting value first.

Radial Dilution

Maximum wall temperature. A typical unsteady streamwise distribution of the wall temperature for a radially diluted rod ($a = 0.7$) is shown in Figure 8*c*. The same phenomenon, as for the axially diluted rod, of slightly shifting the maximum toward the center, is revealed. Figure 9*a* shows the temporal variation of the maximum wall temperature for the various radial diluent additions using dimensionless parameters while Figure 9*b* shows the same figure in dimensional form. Even though the curves in Figure 9*a* are near each other in the corresponding range of t^*, the actual times corresponding to a dimensionless wall temperature value are different. This is because, for a certain value of t^*, the value of t depends on a. In order to further clarify Figure 9*a*, its dimensional counterpart is depicted in Figure 9*b*. From the figure, the great increase in time delay before melting with increasing values of a is obvious. This confirms once more the effectiveness of radial dilution in acting as an in-core heat sink and in improving the safety of the reactor based solely on its inherent safety features.

Further, the time required for the maximum wall temperature to reach a certain value is seen to increase with increasing values of a and to be approximately inversely proportional to the square of the outer diameter. For example, varying a from 0 to 0.7 yields the ratio $(d_{o(a=0.7)}/d_{o(a=0)})^2 = 1.9$, which approximately equals the ratio of maximum wall temperature at $a = 0$ to that at $a = 0.7$ ($\theta_{w\,max(a=0)}/\theta_{w\,max(a=0.7)} = 2.1$) at $t^* = 0.054$. The slight differences among the curves in Figure 8*a* may be attributed to variations in the thermal properties of the cladding material with temperature (note that $t^* = t\alpha/d_o^2$).

Figure 9*c* shows that the distribution of diluent has negligible effects on decreasing the maximum wall temperature during transient operation for the same reasons stated in the steady state analysis section. Varying the diluent material and, consequently, the diluent thermal properties, however, proved to have a considerable effect on the value of the maximum wall temperature (Figure 9*d*) due to the different thermal diffusivities of the materials (Table 3). Materials of higher thermal diffusivities (UO_2 and graphite) show lower wall temperatures than those of lower thermal diffusivities (Al_2O_3 and SiC).

Table 3. Average thermal diffusivities of various diluent materials

Material	α, m^2/s
UO_2	7.28×10^{-7}
Graphite	9.4×10^{-7}
Al_2O_3	9.8×10^{-8}
SiC	1.9×10^{-7}

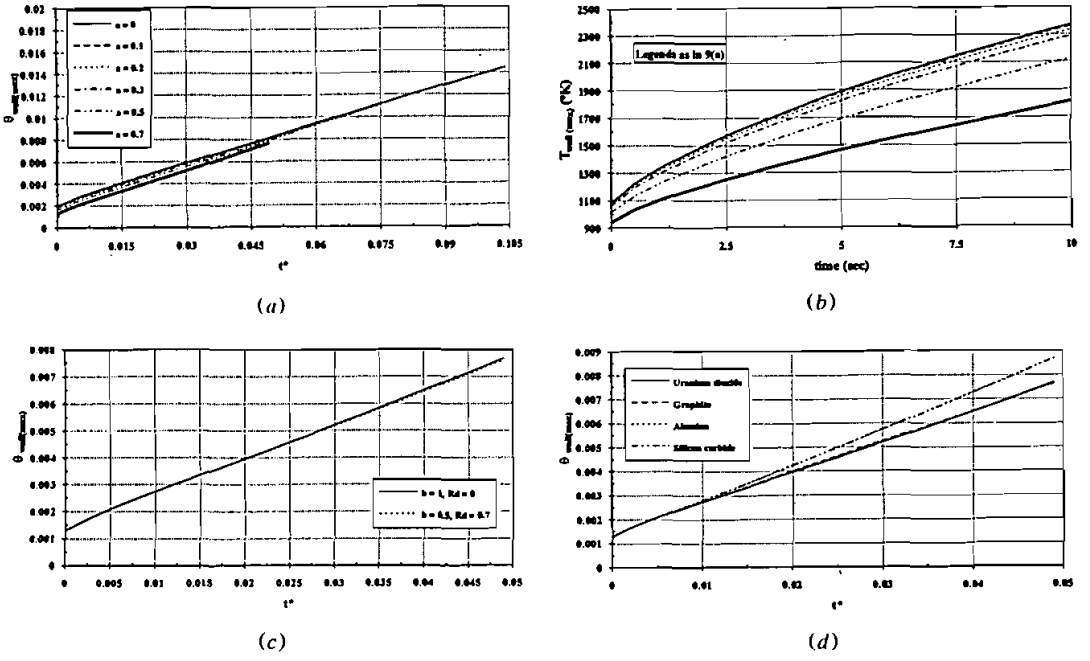

Figure 9. Variation of (*a*) dimensionless and (*b*) dimensional maximum wall temperatures with time for radially diluted rods (central dilution). Variation of maximum wall temperature with time for (*c*) central and central-and-strip radial dilutions and (*d*) central radial dilution using different diluent materials ($a = 0.7$).

Maximum fuel temperature. The streamwise distribution of the fuel centerline temperature is depicted in Figure 10*a* and shows, as anticipated, a shift of the maximum toward the center. Figure 10*b* displays the variation of the maximum fuel centerline temperature with time (t^*) for the various diluent additions. A better improvement than that experienced by the wall temperature is noticed (as compared with the nondiluted rod), which is expected due to (1) better steady state performance and (2) the initial small rates of increase due to initial low wall temperatures. Consequently, the improvement in the fuel centerline temperature overrides the ratio of the diameters squared defined in the previous section.

The diluent thermal diffusivity also affects the value of the maximum fuel centerline temperature (Figure 10*c*), the uranium dioxide and graphite showing better performance. Even though redistributing the radially added diluent using central and strip practices for $a = 0.7$ resulted in higher maximum fuel temperature under steady conditions, during unsteady performance (Figure 10*d*), this difference decreases with time until the two curves merge.

CONCLUSION

The thermal performance under steady and unsteady conditions of axially and radially diluted nuclear fuel cells was investigated numerically. Results generated indicate that axial dilution has a negligible effect on reducing the maximum

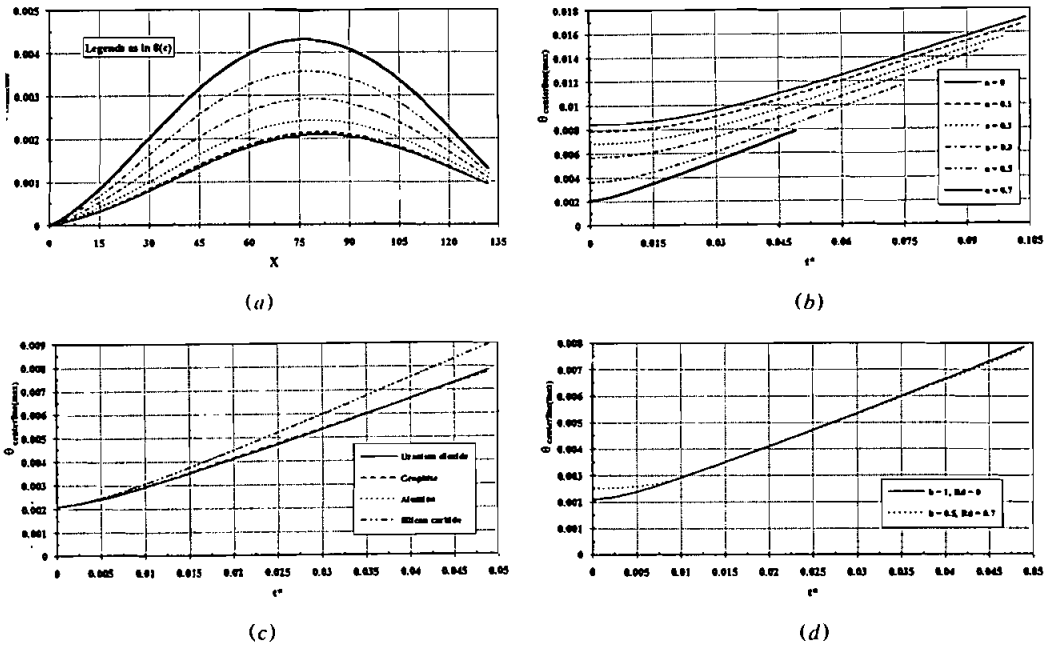

Figure 10. (*a*) Transient axial distribution of centerline temperature in radially diluted rods ($a = 0.7$, central dilution). Variation of dimensionless maximum centerline temperature with time for (*b*) radially diluted rods (central dilution), (*c*) radially diluted rods using different diluent materials ($a = 0.7$, central dilution), and (*d*) radially diluted rods using central and central-and-strip radial dilution practices ($a = 0.7$).

fuel and wall temperatures of the fuel rod during steady performance and on increasing the time delay before melting during unsteady operations. As such, its implementation is not recommended. On the other hand, radial dilution shows a great reduction in these temperatures during steady operation and a noticeable increase in time delay before melting under unsteady conditions. Thus, this configuration enhances the safety of the reactor, and its use is strongly recommended. Finally, whether such fuel rods can economically be manufactured remains an open question for the industry to answer.

REFERENCES

1. R. Hannerz and M. Pederson, PIUS—The Nuclear Reactor of Tomorrow, *Nucl. Eng.*, vol. 32, no. 5, pp. 162–171, 1991.
2. A. E. Waltar and A. B. Reynolds, *Fast Breeder Reactors*, Pergamon, New York 1981.
3. J. Weisman, *Elements of Nuclear Reactor Design*, Elsevier Scientific, Amsterdam, 1977.
4. J. R. Lamarsh, *Introduction to Nuclear Engineering*, Addison-Wesley, Reading, Massachusetts, 1983.
5. W. B. Kemmish, Gas-Cooled Fast Reactors, *Nucl. Energy J. BNES*, vol. 21, no. 1, 1982.
6. R. H. S. Winterton, *Thermal Design of Nuclear Reactors*, Pergamon, New York, 1981.

7. H. Schlichting, *Boundary Layer Theory*, 7th ed., pp. 475–531, McGraw-Hill, New York, 1960.
8. F. Moukalled, J. Kasamani, and S. Acharya, Turbulent Convection Heat Transfer in Longitudinally Conducting Externally Finned Pipes, *Numer. Heat Transfer Part A*, vol. 21, pp. 401–421, 1992.
9. J. Nikuradse, Gesetzmässigkeit der turbulenten Strömung in glatten Röhren, *Forschungshet*, p. 356, 1932.
10. E. R. Van Driest, On Turbulent Flow near a Wall, *J. Aero. Sci.*, vol. 23, pp. 1007–1011, 1956.
11. S. V. Patankar and D. B. Spalding, *Heat and Mass Transfer in Boundary Layers*, Intertext Books, London, 1970.
12. S. V. Patankar, *Numerical Heat Transfer and Fluid Flow*, Hemisphere, New York, 1980.
13. J. P. Holman, *Heat Transfer*, McGraw-Hill, New York, 1989.
14. T. S. Rohsenow and S. W. Choi, *Heat, Mass, and Momentum Transfer*, Prentice-Hall, Englewood Cliffs, New Jersey, 1961.